Splitting of Cyclobutane-Type Uracil Dimer Cation Radicals. Hartree−Fock, MP2, and Density Functional Studies

Janusz Rak,† Alexander A. Voityuk, and Notker Rösch*

Lehrstuhl für Theoretische Chemie, Technische Universität München, D-85747 Garching, Germany

Received: March 27, 1998; In Final Form: June 24, 1998

The cation pathway of the cyclobutane-type uracil dimer cycloreversion process has been studied using various quantum chemical methods. Taking into account dynamic correlation effects (using B3LYP and MP2 calculations), we found that, after ionization of the parent neutral dimer, the uracil dimer cation radical dissociates spontaneously. The lack of any activation barrier for the splitting reaction is in good agreement with the extremely low stability of uracil dimer cations found experimentally. Hartree−Fock (HF) calculations predict two reaction pathways for the splitting process. The existence of these paths is associated with the conformational flexibility of the intermediate in which the two uracil rings are connected by the remaining C5−C5′ bond. To gain more detailed insight into effects of dynamic correlation on the cycloreversion reaction, all stationary points found at the HF level were also analyzed using B3LYP and MP2 methodology. Effects of a polar environment on the cleavage process were explored using the self-consistent reaction field method. In our model study, we also considered the influence of structural constraints in DNA on the dimer cation splitting.

Introduction

Pyrimidine dimers are among the most common photoproducts found in genetic material that has been exposed to UV radiation.[1−6] These moieties are formed in a photochemically allowed cycloaddition reaction between pyrimidine bases located at adjacent positions on a DNA strand. These defects may cause lethal effects by blocking replication and transcription in living cells.[5] To repair such damage, nature created special types of enzymes dubbed photolyases,[3,4] which recognize photodimers and, utilizing light from the near-UV and visible regions (360−460 nm), initiate electron transfer that leads to the cleavage of these dimers. For several model systems containing photooxidizing or photoreducing sensitizers it has been shown experimentally that cycloreversion can occur via alternative reaction pathways that involve either dimer radical cations or anions.[7,8] Recent experimental studies on systems that contain photodimers as well as the cofactor $FADH^-$ (also used by photolyases) suggest that the formation of radical anions initiates dimer cleavage.[9,10] Semiempirical and ab initio calculations reveal a distinctive decrease in the activation barrier for splitting after reduction of the dimer.[11,12]

Recently rhodium(III) complexes incorporated in DNA[13] have been reported to play a catalytic role in the photorepair of thymine dimers. An oxidizing excited state of the rhodium complex formed after irradiation at 400 nm causes cycloreversion in this system to proceed via the dimer radical cation. In light of these findings, the cation pathway of dimer photocleavage also becomes important. This motivated us to carry out a computational study of the splitting reaction of pyrimidine dimer cations.

Two other ab initio studies have so far been published on the pyrimidine dimer radical cations.[14,15] The first work deals with the electronic structure of dimers.[14] Very recently, while the present work was in progress, a complete active space (CAS) SCF study of the fragmentation mechanism of thymine dimers has been presented in which various stationary states have been located along the path of the splitting reaction.[15] However, a rather limited active space (three electrons, four orbitals) was used in that CASSCF analysis; thus, no dynamic correlation effects, which are important for a reliable description of such systems, were taken into account.[15] Moreover, on the basis of occupation numbers of orbitals used in CASSCF calculations, the authors of this study conclude that the "reaction is essentially well described by a single determinant".[15] A very similar conclusion concerning the quality of a single-determinant description was reached by Jungwirth et al.[16] in their study of the cyclobutane radical cation; they found one leading configuration to account for more than 94% of the MCSCF expansion at all stationary points on the corresponding potential-energy surface (PES). Thus, the (3,4) CASSCF results for the splitting reaction of pyrimidine dimer cation are expected to be very similar to those obtained at the unrestricted Hartree−Fock (UHF) level employed in the present study as a first approximation; we shall see that this is indeed the case.

Since inclusion of dynamic correlation effects is essential when a reaction profile is studied, we decided to go beyond the UHF level in our investigation of the dimer splitting reaction. First, we "corrected" the PES at the UHF stationary points by single-point calculations at the MP2 and density functional (DF) levels of theory. Several recent studies[17−22] of organic systems and their reactions concluded that DF methods,[23] the hybrid B3LYP method[24−26] in particular, provide an accurate approach for determining molecular structures and energetics including reaction activation barriers. Second, since this computational procedure is more accurate and less demanding than an MP2 approach,[27] we also performed geometry optimizations at the B3LYP level to localize stationary points of the corresponding improved PES.

* To whom correspondence should be addressed.
† On the leave from the Department of Chemistry, University of Gdansk, Sobieskiego 18, 80-952 Gdansk, Poland.

S1089-5639(98)01665-X CCC: $15.00
Published on Web 08/14/1998

Furthermore, we estimated the influence of a polar medium on the reaction profile of the dimer splitting, using self-consistent reaction field (SCRF) calculations at the B3LYP level. Thus, the present study focuses on modeling the splitting of a pyrimidine dimer radical cation in the gas phase and in solution. In this way its emphasis differs from that of the CASSCF study mentioned above.[15] However, to increase the realism of our model investigations for the splitting of photodimers in DNA, we also performed B3LYP geometry optimizations where constraints of the process in DNA were taken into account.

Method

We chose the uracil dimer as a model for the pyrimidine dimer cleavage. Furthermore, we assumed the dimer to be in a cis−syn configuration, in agreement with the experimental finding that this isomer is the most abundant pyrimidine photoproduct when DNA is exposed to UV radiation.[3]

All molecular orbital calculations were carried out with the help of the program Gaussian94.[28] Stationary points for the splitting process were located at the UHF level, employing the 6-31G* basis set.[29] Along the reaction path, UHF wave functions were checked for spin contamination which turned out to be relatively small since the expectation values of $\langle S^2 \rangle$ never exceeded 0.82. However, several states suffering from spin contamination were also generated. Therefore, energies for projected wave functions were compiled for the comparison.

The quality of the basis set used in the calculations is an important issue. To check the saturation of the basis set for the problem under consideration, we used four different basis sets, 6-31G*, 6-31G**, 6-311G*, and 6-311G**,[28] to evaluate the energy of the splitting reaction. The various values of the reaction energy differed at most by 2.3 kcal/mol. Since the smallest basis set with 256 basis functions comprises 80 functions less than the biggest one, we settled for the 6-31G* basis set.

No constraints were applied during the geometry optimizations, which were carried out with the help of the Berny algorithm.[30,31] Transition states were located by first employing the reaction coordinate method followed by a gradient minimization.[30] We checked located stationary points by a harmonic frequency analysis,[32] and we used these vibrational frequencies after proper scaling[32] to evaluate zero-point energies (ZPE).

In the DF calculations we employed the Becke three-parameter hybrid functional (B3LYP)[24,25] combined with the correlation functional of Lee, Yang, and Parr.[26] The 6-31G* basis set was used for the wave-function-based calculations as described above. Here, we refrained from applying spin projection, as the expectation value of $\langle S^2 \rangle$ was at most 0.76, thus exhibiting essentially no deviation from the ideal value.

The basis set superposition error for the product complex was estimated using the standard counterpoise procedure.[33]

Finally, we estimated the effect of a polar solvent (water, dielectric constant $\epsilon = 78.4$) on the reaction energetics within the self-consistent reaction field approach[34] using a spherical cavity model as implemented in Gaussian94.[35] For each molecular system the cavity radius was determined from the volume inside the surface of constant electron density of 0.001 au.

Results and Discussion

On the Modeling Strategy Adopted in the Work. Before presenting the results, we would like to comment on methodological and model-building aspects of this work.

As for the methodological thrust of this study, we aimed at elucidating the role of dynamic correlation effects in the description of the cation dimer splitting process. (Note that dynamic correlation effects were not taken into account in a recent CASSCF study of dimer cation splitting.[15]) We shall start with a discussion of Hartree−Fock results, which we will supplement by results from calculations based on MP2 and DFT methodology. In this way, we will show that the reaction profile of the splitting of a pyrimidine dimer cation is crucially affected by dynamic correlation effects. In particular, we will demonstrate that the splitting process proceeds activationless at the correlated levels while two small barriers are found in HF and CASSCF[15] calculations. Nevertheless, we believe that the changes in geometries of the system from the nonrelaxed cation to the product complex will, at least to a good approximation, follow the HF path and that the splitting process indeed proceeds in a nonconcerted fashion as already found at this level. Thus, it seems worth describing the structural transformations that make up the cleavage process at the HF level, although the HF energetics needs corrections.

As pointed out in the Introduction, this work focuses on the splitting reaction of *free* model dimers, just as recent experimental studies do.[8−10] Thus, in the major part of the work, the splitting process will be considered without any structural constraints. Solvent effects on the energy profiles will also be taken into account, since the experimental studies were carried out mainly in aqueous solutions. However, in our dimer model study, we shall also discuss the effect of structural constraints in DNA on the dimer cation splitting in order to gain insight into the cation cleavage reaction as it proceeds in DNA.

Structural Transformation During the Cycloreversion Process. Let us start with a discussion of the structural transformation as obtained at the HF level. Later on, this approximate picture of the reaction path will be corrected according to calculations that include correlation effects. Figure 1 shows the structures of stationary points found at the UHF level along the reaction path of the conversion of the dimer cation to separated monomers. Pertinent geometric parameters are collected in Table 1. Assuming vertical ionization of the dimer, the splitting reaction starts from the nonrelaxed structure $U<>U^+_{NR}$; the geometry of this species is identical to that of the neutral dimer U<>U. Relaxation of $U<>U^+_{NR}$ results in $U<>U^+$. Thereby, the most significant structural change is the elongation of the distance C6−C6′ (Figure 1) from 1.55 Å in $U<>U^+_{NR}$ to 2.14 Å in $U<>U^+$ (Table 1). To elucidate the underlying change in the electronic structure, it is helpful to inspect the HOMO of the neutral dimer. It is strongly localized on the bond connecting atoms C6 and C6′. The corresponding bonding interaction decreases once this level is ionized in the neutral dimer, thus rationalizing the substantial elongation of the C6−C6′ distance. The other bonds of the four-membered ring change very little. Therefore, the almost equilateral structure of the four-membered ring of the neutral dimer becomes trapeziodal in $U<>U^+$, while its puckering remains almost unchanged.

The fact that the structure of $U<>U^+$ found at the SCF and CASSCF levels[15] exhibits such an extremely long C6−C6′ bond distance in the intermediate 1 (INT1) while the corresponding bond C5−C5′ remains almost unchanged suggests that the dissociation of the cation proceeds in a stepwise manner. Indeed, we were able to locate transition states TS1 and TS4, respectively, associated with the stepwise breaking of these two bonds of the four-membered ring. The first one, TS1, interconnects the structures $U<>U^+$ and INT1 (Figure 1). The structure

TABLE 1: Geometric Parameters of the Four-Membered Ring of the Uracil Dimer Cation for Stationary Points During the Splitting Reaction Calculated at the UHF/ 6-31G* Level (distances in Å, Angles in deg)

	ring	U<>U$^+_{NR}$	U<>U$^+$	TS1	INT1	TS2	INT2	TS3	TS4
				Bond Distances					
C5−C5′		1.553	1.560	1.560	1.548	1.567	1.566	1.944	1.932
C5′−C6′		1.539	1.516	1.515	1.501	1.502	1.501	1.413	1.417
C6′−C6		1.553	2.139	2.174	3.261	3.644	3.810	3.918	3.394
C6−C5		1.537	1.511	1.510	1.480	1.482	1.504	1.428	1.419
C6−N1	1	1.429	1.326	1.316	1.276	1.276	1.285	1.302	1.303
	1′	1.441	1.338	1.345	1.386	1.391	1.392	1.353	1.357
				Dihedral Angles					
C6′−C5′−C5−C6		−20.7	−21.8	−23.2	−79.8	−121.2	−213.9	−181.5	−79.9
H5−C5− C4−C6	1	130.1	122.7	122.1	114.4	113.4	117.8	136.3	137.0
	1′	−126.5	−122.7	−122.7	−120.1	−116.3	−118.3	−136.3	−134.3
H6−C6−N1−C5	1	−126.2	−156.1	−159.2	−177.3	−178.4	−169.7	177.1	176.8
	1′	131.7	157.4	156.6	146.4	144.9	145.3	−172.6	−174.8

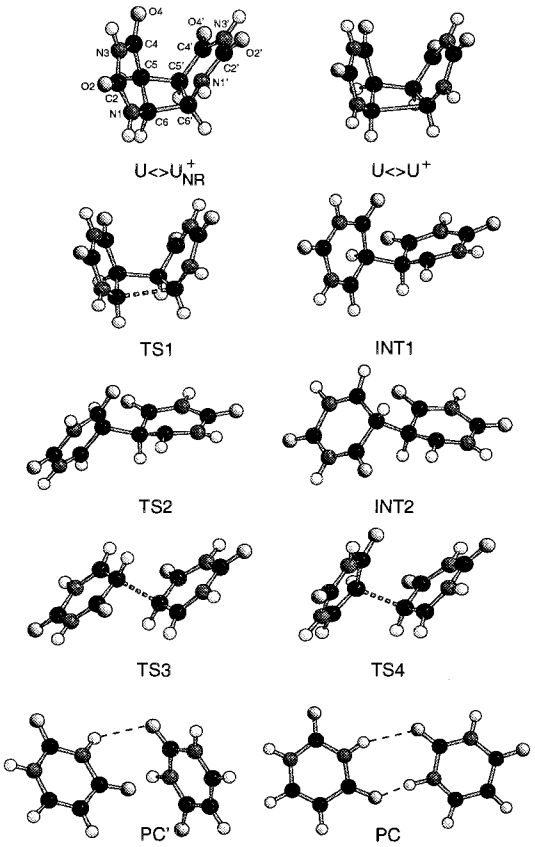

Figure 1. Pertinent structures of the uracil photodimer radical cation along the path of the splitting reaction, calculated at the UHF/6-31G* level: U<>U$^+_{NR}$—nonrelaxed photodimer cation; U<>U$^+$—relaxed photodimer cation; TS1—saddle point connecting U<>U$^+$ and intermediate; INT1—intermediate 1; TS2—saddle point connecting INT1 and INT2; INT2—intermediate 2; TS3—saddle point connecting INT2 and product complex; TS4—saddle point connecting INT1 and product complex; PC′—T-shape product complex; PC—planar product complex.

TS1 is in general very similar to that of U<>U$^+$ (Table 1) with the C5−C5′ bond almost unchanged. Only the C6−C6′ bond distance increases during this step, to 2.174 Å in TS1 (Table 1); also, the absolute value of the dihedral angle C6′−C5′−C5−C6 increases further. Such small differences in the geometrical parameters suggest a very small barrier for the transformation and thus a considerable instability of pyrimidine radical dimers at variance with the stable neutral dimers.

The C6−C6′ bond is cleaved in the intermediate INT1 (Figure 1), and its length increases to 3.261 Å (Table 1). The opening of the four-membered ring is accompanied by a simultaneous rotation of the pyrimidine rings around the C5−C5′ bond relative to each other; the dihedral angle C6′−C5′−C5−C6 reaches −79.8° in INT1. At the same time the dihedral angle H6−C6−N1−C5 (ring 1) approaches 180° (Table 1), which demonstrates a distinctive increase in the degree of sp^2 hybridization at the center C6 of ring 1. Concomitantly, the dihedral angle H6′−C6′−N1′−C5′ decreases from 157.4° in U<>U$^+$ to 146.4° in INT1 (Table 1), indicating a hybridization change at the center C6′ toward sp^3. This analysis is supported by changes in the corresponding bond lengths. The distance C6−N1 decreases from 1.326 Å in U<>U$^+$ to 1.276 Å in INT1, while the distance C6′−N1′ increases from 1.338 to 1.386 Å (Table 1). These structural changes during the transformation from U<>U$^+$ to INT1 are accompanied by spin and charge transfer; we will comment on them in the section on solvent effects.

During the next step of the reaction, the intermediate INT1 separates into two uracil monomers—one charged, one neutral (path I). The structure of transition state TS4 relating to this transformation is shown in Figure 1. Again, the most striking structural change from INT1 to TS4 relates directly to the bond C5−C5′,which is to be broken (Table 1); it is elongated by 0.38 Å relative to its value in INT1.

Furthermore, we have considered an alternative way of transformation to the monomers (path II) that takes the conformational flexibility of intermediate INT1 into account. Namely, further rotation of pyrimidine rings of INT1 around the C5−C5′ bond relative to each other leads to the new conformation, INT2 (see Figure 1). The main structural difference between INT1 and INT2 is characterized by the dihedral angle C6′−C5′−C5−C6, which decreases from −79.8° in the former conformation to −213.9° in the latter (Table 1). Transition state TS2 separates INT1 and INT2 (Figure 1); the structure of TS2 is quite similar to those of INT1 and INT2, with the exception of the dihedral angle C6−C5−C5′−C6′ being −121.2° (Table 1).

INT2 splits into monomers via transition state TS3 (Figure 1); the structure of TS3 resembles that of TS4. The most noticeable changes when moving from INT2 to TS3 are the elongation of the C5−C5′ bond and the increase in planarity of both rings.

One should, however, keep in mind that reaction path II is feasible only for a free dimer. In DNA, conformational constraints resulting from the presence of the backbone and the complementary strand make a rotation of the pyrimidine rings relative to each other very difficult and should thus prevent the formation of INT2.

The neutral uracil molecule and its cation, which result from the separation of the intermediates, form an ion−dipole complex. We found two structures of this product complex (PC, Figure 1). The first structure, PC′, is T-shaped with both rings

TABLE 2: Reaction Energies[a] ΔE for Elementary Processes Involved in the Splitting of Uracil Dimer Radical Cations and, Where Appropriate, Activation Energies[a] E_a toward the Corresponding Transition-State Structures as Calculated at Various Levels of Theory

	UHF/6-31G*[b]		MP2/6-31G*[b]		B3LYP/6-31G*[b]		SCRF/B3LYP/6-31G*[b]	
process	ΔE[d]	E_a[d]	ΔE[d]	E_a[d]	ΔE	E_a	ΔE	E_a
U<>U^+_{NR} → U<>U^+	−18.40 (−7.78)		−38.48 (−29.38)		−16.70		−18.70	
U<>U^+ → INT1	−13.10 (−13.53)	0.02 (−0.02)	2.05 (1.82)	0.88 (0.84)	−0.32	0.13	−4.00	−1.05
INT1 → PC′	−15.49 (−15.45)	9.65 (7.53)	7.85 (7.89)	−1.84 (−3.75)	−10.66	−6.58	−4.35	−3.62
INT1 → PC	−29.36 (−39.21)		−12.47 (−21.16)		−29.20		−22.01	
INT1 → INT2	−7.17 (−7.12)	3.18 (3.20)	−6.33 (−6.31)	4.43 (4.44)	−5.36	5.75	0.21	7.09
INT2 → PC′	−8.32 (−8.33)	9.67 (7.58)[e]	14.18 (14.20)	−1.48 (−3.31)[e]	−5.30	−7.38[e]	−4.56	−5.58[e]
INT2 → PC	−22.19 (−32.09)		−6.14 (−14.85)		−23.84		−22.22	
PC′ → U + U^+	13.54 (4.12)		11.36 (3.04)		13.75		0.15	
PC → U + U^+	27.40 (27.89)		31.68 (32.09)		32.29		17.81	
U<>U^+_{NR} → U + U^+	−33.46 (−32.64)		−17.22 (−16.62)		−13.93		−26.90	

[a] In kcal/mol. [b] Geometry at UHF/6-31G* level. [c] Self-consistent reaction field model for water as solvent. [d] Energies after spin projection given in parentheses [e] Barrier connected with the splitting of the C5−C5′ bond.

perpendicular to each other (Figure 1). Overall, relatively small changes of INT1 or INT2 are required to reach PC′. The second structure, PC, is planar; it is a good candidate for the global minimum, since it features an advantageous mutual orientation of the dipole moment of neutral uracil and the charged monomer cation as well as two relatively strong intermonomer hydrogen bonds. Note, however, that these two configurations of the product complex are not possible in DNA because H1 is not present in pyrimidine bases when they are incorporated in a double helix, although they may be important for the interpretation of experimental results on model compounds in solutions.[7,8]

The structural transformation of the uracil dimer radical cation described above was based on UHF data; for path I, the results are quite similar to those obtained by Aida et al.,[15] despite the fact that different models (uracil vs thymine dimer) and different methods (UHF/6-31G* vs CASSCF/6-31G) were used. Differences in bond lengths for comparable structures do not exceed 8%, being below 1% in many cases. In a relative sense, the largest structural deviation is calculated for the C5−C5′ bond of INT1; at the UHF level it exhibits a length rather typical for a C−C single bond, 1.55 Å (Table 1), but the CASSCF value is 0.13 Å longer.[15] Overall, these findings corroborate that a single-determinant wave function as used in this study provides a very satisfactory description for the cleavage of pyrimidine dimer cations. The single-determinant description, which underlies the Kohn−Sham procedure for a DF treatment, is therefore expected to be rather reliable for the reaction under investigation.

Thus, it seems natural to take dynamic correlation into account by following up the UHF calculations with a DF treatment of the stationary points of the PES. We were surprised to discover that B3LYP optimizations (starting from various geometries, either the unrelaxed dimer cation structure U<>U^+_{NR} or, at the UHF level, the relaxed dimer U<>U^+ and the intermediate (INT1) did not converge to the corresponding cation geometries but resulted directly in the structure of the product complex PC′ (Figure 1). Thus, the structures U<>U^+, TS1, INT1, and TS4 found at the HF (or CASSCF) level do not correspond to stationary points at the DF level. This important finding is a harbinger for the correlation effects on the energy profile of the splitting reaction, which we will discuss in detail in the following section. On one hand, it underlines the crucial role of dynamic correlation in the description of the PES of the reaction considered. On the other hand, it indicates the lack of any kinetic barrier, when the cleavage reaction proceeds along reaction path I. This result is in line with experiments that found an extreme instability of the model dimer cation, the maximum lifetime being in the range of 10^{-10}−10^{-9} s for nonbridged dimer cations and longer than 10^{-9} for bridged dimer cations.[8]

Energetics of the Photodimer Cation Splitting. In this section we consider how the correlation energy influences the PES established at the Hartree−Fock level. We will start with the UHF description of the energy profile. Next, this profile will be compared to those obtained when corrected by single-point MP2 and B3LYP calculations. This "perturbation" procedure allows one to rationalize the calculated differences between HF and correlated results. Furthermore, we will gain chemical insight into the various stages of the splitting reaction, which would be very difficult to obtain directly if we had to rely on the B3LYP PES only.

The results of the MP2//UHF and B3LYP//UHF energy analyses are collected in Table 2 and compared to results from other computational approaches. To facilitate a comparative visualization of the reaction profile, we present in Figure 2 relative energies of the various structures, using U<>U^+_{NR} as a reference. We start with a discussion of the UHF energy profile.

According to UHF, U<>U^+_{NR} relaxes without any barrier to U<>U^+, releasing 18.4 kcal/mol; this energy is reduced to 7.8 kcal/mol if a spin-projected wave function is used (Table 2). In turn, the relaxed cation is transformed exothermically into the intermediate product INT1 (Figure 2A). This transformation exhibits a tiny (formal) activation barrier of 0.02 kcal/mol (Table 2). The existence of an activation barrier between U<>U^+_{NR} and INT1 was also pointed out by Aida et al.[15] who calculated a value of 0.26 kcal/mol at the CASSCF level. The difference between these two results is probably connected to the lack of polarization functions in the basis sets of the latter study.[15] Indeed, we calculated a barrier of 0.37 kcal/mol at the UHF/3-21G level. Anyway, barriers of this size are of no importance for chemical systems. In the present case, the barrier disappears if one takes zero-point energies into account. Thus, even at the HF level the cation is unstable toward transformation into the intermediate structure INT1.

The next step of the dimer splitting, the transition from INT1 to PC (path I), is also exoenergetic; the corresponding energy changes ΔE are −15.5 and −29.4 kcal/mol for PC′ and PC, respectively (Table 2). At the UHF level the dissociation of INT1 is associated with a kinetic barrier of 9.7 kcal/mol (or 7.5 kcal/mol at the spin-projected level; see Table 2). Aida et al.[15] obtained a value of 1.4 kcal/mol for this barrier; the difference between the present UHF and their CASSCF results is due to the relatively high energy of INT1 calculated at the CASSCF level. Indeed, the energy difference between U<>U^+ and TS4 is found to be in good agreement at the HF and

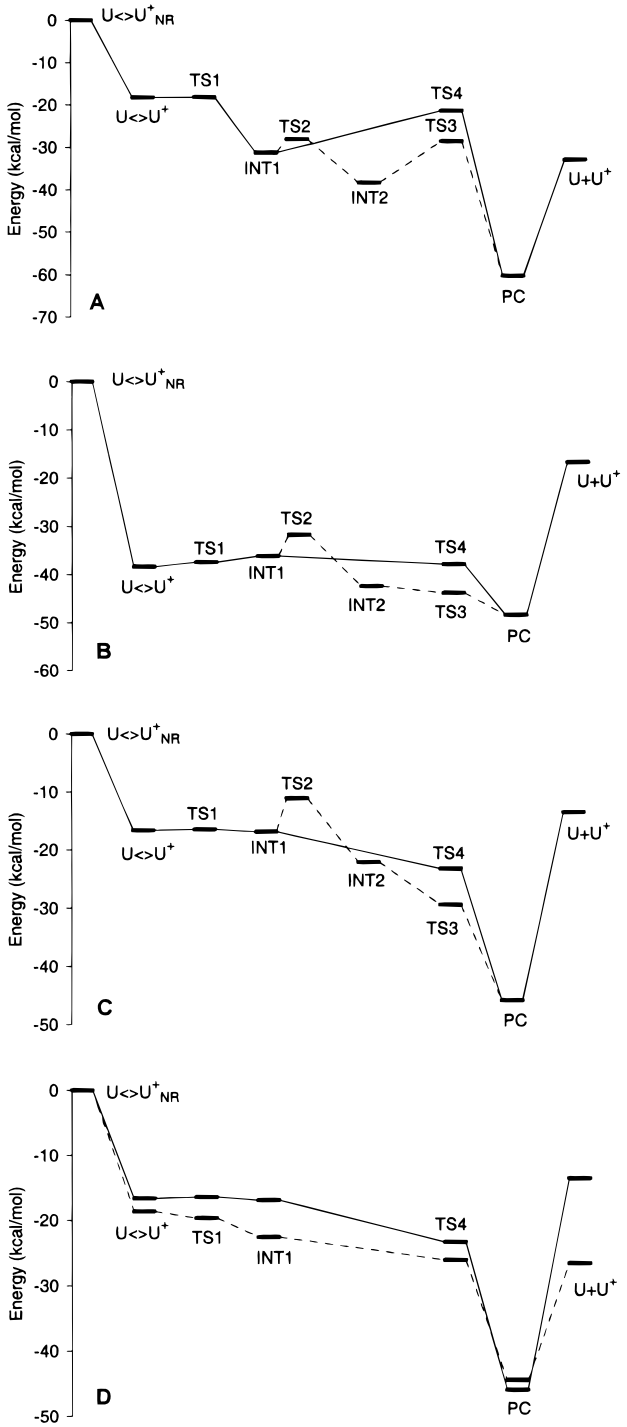

Figure 2. Relative energies of UHF/6-31G* stationary structures along the path of the splitting reaction of the uracil dimer cation, calculated at various levels of theory: (A) UHF/6-31G*, (B) MP2/6-31G*, (C) B3LYP/6-31G* (solid lines—reaction path I, dashed lines—reaction path II); (D) SCRF/B3LYP/6-31G* (dashed lines—path I), B3LYP/6-31G* (solid lines—path I).

CASSCF levels, 3.5 and 3.1 kcal/mol, respectively.[15] Thus, a reinvestigation of the structure and energy of INT1 at the CASSCF level seems to be desirable (recall the rather long bond distance C5−C5′ mentioned above).

Along the alternative path II where INT1 undergoes a rotation around the C5−C5′ bond this transformation is accompanied by an activation barrier of 3.2 kcal/mol (Table 2). The subsequent stationary point INT2 is 7.2 kcal/mol more stable than INT1. From there, the dimer cation separates into monomers via an activation barrier (TS3) of 9.7 kcal/mol (Table 2).

TABLE 3: Solvation Energies, Mulliken Charges q, q', spin densities σ, σ' of Each Ring (1 and 1′, Respectively) and Dipole Moments of the Uracil Dimer Radical Cation at Various UHF Stationary Points of the Splitting Reaction

point[a]	solvation energy[b]	charge density[c]		spin density[c]		dipole moment[d]
		q	q'	σ	σ'	
U<>U^+_{NR}	−37.59	0.46	0.54	0.41	0.59	6.84
U<>U^+	−39.59	0.52	0.48	0.48	0.52	8.14
TS1	−40.77	0.54	0.46	0.46	0.54	8.18
INT1	−43.27	0.72	0.28	0.17	0.83	8.87
TS2	−41.93	0.81	0.19	0.02	0.98	8.84
INT2	−37.70	0.73	0.27	0.01	0.99	4.60
TS3	−35.90	0.54	0.46	0.47	0.53	0.47
TS4	−40.31	0.53	0.47	0.45	0.55	7.29
PC′	−36.96	0.32	0.68	0.30	0.70	5.70
PC	−36.08	0.23	0.77	0.12	0.88	5.64
U + U^+	−50.56	0.00	1.00	0.00	1.00	9.89[e]

[a] Geometry at UHF/6-31G* level. [b] In kcal/mol, including the Born charge term.[35] [c] In au. [d] Calculated at the B3LYP/6-31G* level, in debye. [e] Sum of the contributions from U, 4.12 D, and U^+, 5.77 D.

The complex PC is stabilized by two rather strong hydrogen bonds and thus has a lower energy than PC′. At the HF level, the stabilization energies relative to the noninteracting monomers are −13.5 and −27.4 kcal/mol for PC and PC′, respectively (Table 2). As a result of the fact that a cation (with a relatively compact charge cloud) is involved in this system, the basis set superposition error is quite small, amounting to only 1.7 and 1.8 kcal/mol for PC and PC′, respectively. Therefore, we refrained from applying any such correction to the values presented in Table 2.

From this description of the energy hypersurface at the HF level (Figure 2A) it seems as if path II represents the preferred way for splitting a cyclobutane-type uracil dimer cation radical, since the transition states TS2 and TS3 require less energy expense (relative to INT1) than TS4 of path I. However, we have already stressed that a description of the reaction profile without electron correlation effects is only approximate. This point is supported by the rather different geometry optimization results at the HF and B3LYP levels mentioned in the previous section. Now we turn to a discussion of the two "corrected" representations of the reaction path, generated by single-point calculations at B3LYP and MP2 levels for all HF stationary points (Table 2).

First, note the significant change in the overall shape of the reaction profile, which emphasizes the importance of *dynamic* correlation effects (cf. part A to parts B and C of Figure 2). The MP2 and B3LYP profiles are qualitatively similar, but the latter lies at a less negative energy in comparison to the MP2 estimates, which, as found in many cases, seem to be overcorrected here as well. (Note the different energy scales of Figure 2, parts B and C.) In strong contrast to the HF picture, one notices a very flat region when moving along path I from U<>U^+ to TS4 (cf. part A to parts B and C of Figure 2). Actually, at the MP2 level, INT1 lies at a higher energy than both UHF transition-state structures TS1 and TS4. Also, the (direct) barriers connecting INT1 and INT2 to PC disappear completely. For INT1 this was anticipated by the full geometry optimization at the B3LYP level. Full geometry optimization of INT2 at this DF level leads to the formation of a locally stable cyclic structure in which two uracil rings are also connected by a C6−O4′ bond, which forms by interaction between an electron pair localized on O4′ and the empty p orbital localized on C6 (see the charge on ring 1; Table 3). At the B3LYP-corrected surface (single-point B3LYP energies calculated for HF geometries) this structure is only 1.6 kcal/mol more

stable than INT2. On the other hand, the fact that the barrier related to TS3 (cf. parts A and C of Figure 2) disappears also shows the instability of INT2 toward C5−C5′ bond cleavage. Thus, the reaction following path II will also lead to the product complex, since the cyclic structure is (likely) too shallow a minimum to stop the process, at least at the room temperature.

The full B3LYP optimization demonstrates also the lack of any barrier between U<>U$^+$ and INT1. This may be due to the tendency of such ring systems to rotate relative to one another at a correlated level of theory, as pointed out in a study of the stacking energy of nucleic acid base pairs.[36] The only barrier that remains at the correlated level of theory is that between INT1 and INT2, associated with transition state TS2. In fact, this barrier even increases at the correlated level (HF, 3.2; MP2, 4.4; B3LYP, 5.8 kcal/mol (see Table 2). This finding suggests that the splitting reaction should proceed via path I rather than via path II although INT2 is more stable than INT1.

The strategy used so far, to optimize geometries at the UHF SCF level followed by single-point calculations at a correlated level, is adequate provided that the relative energies of the stationary points do not change significantly. Otherwise, one has to carry out a reoptimization at a correlated level to obtain a more realistic picture of the PES. The system under study obviously belongs to the latter category. The results of optimization at the B3LYP level (not displayed in Table 2) seem to be the most reliable ones of the present study. Therefore, the energetic characteristic of the process under consideration can be summarized as follows: abstraction of an electron from a uracil dimer leads to the *immediate* formation of a product complex, accompanied by the release of about 48 kcal/mol. Since the stabilization energy of PC amounts to 33 kcal/mol, the exothermicity of the overall dissociation process of a nonrelaxed pyrimidine dimer to the separated monomers is about 15 kcal/mol. Nevertheless, the detailed study of the PES, based on B3LYP or MP2-corrected energies of UHF stationary structures, should provide a realistic picture of the reaction profile, as it points to the existence of a rather extended "flat" region. As mentioned above, it would computationally be rather costly to obtain this information via a direct study of the internal reaction coordinate at a correlated level of theory.

At this point, it may be of interest to compare the present results to those obtained by the semiempirical AM1 method used in our previous study.[11] Similar to the B3LYP approach, the AM1 method predicts an activationless transformation from U<>U$^+$ to INT1 but finds a barrier (analogous to TS4) between INT1 and PC, which is comparable to the HF result. Aida et al. dismiss the AM1 results, since they fail to reproduce even qualitatively the AM1 fragmentation mechanism at the CASSCF level.[15] Actually, the AM1 method correctly describes the fact that removing an electron from the dimer leads to the immediate splitting of the C6−C6′ bond, whereas the CASSCF calculations[15] predict a local minimum U<>U$^+$ (as does UHF) that exhibits a structure with two pyrimidine bases connected with both the C5−C5′ and the C6−C6′ bonds. As just discussed, the activation barrier TS1 is an artifact of methods that fail to properly account for dynamic electron correlation; rather, the C6−C6′ bond undergoes spontaneous cleavage. This agreement between the AM1 and B3LYP (or MP2) data can be attributed, at least in part, to the fact that the AM1 method as well as other semiempirical schemes incorporates dynamic electron correlation due to the special treatment of two-electron integrals and the choice of semiempirical parameters.[37] Thus, the CASSCF calculations[15] rather than those of AM1 fail to reproduce properly the first fragmentation step of a pyrimidine dimer.

The analysis presented above refers to the free pyrimidine dimer radical cation. In DNA the conformational freedom of pyrimidine bases is limited, for example, neighboring bases are rotated by 36° (10 nucleotide residues per turn). To account for this effect, we carried out restricted geometry optimizations at the B3LYP level. During these optimizations two geometrical parameters that determine the arrangement of the rings relative to each another were fixed: the C5−C5′ distance and the dihedral angle C6′−C5′−C5−C6. Several sets of these two parameters were probed: 1.56 Å, −21.8°; 1.75 Å, −23.5°; 2.0 Å, −25.5°; 2.5 Å, −29.5°. In this way, we tried to mimic the effect of constraints on the splitting process in DNA. It turned out that such constraints lead to a kinetic barrier of about 20 kcal/mol; the highest energy was found for 2.0 Å and −25.5°. The structure corresponding to the high barrier is probably connected to a fully concerted splitting process (with respect to the cyclobutane ring), which is symmetry-forbidden. However, a restricted optimization with the distance C5−C5′ fixed at 2.0 Å and the angle C6′−C5′−C5−C6 at −31° leads to the complete disappearance of the barrier; thus, the value of the barrier is very susceptible to structural details that are difficult to simulate. These results show that the photorepair reaction may be very sensitive to constraints present in DNA, in particular the rotation of the rings relative to each other. Since this rotation is hindered in DNA, the dimer splitting process can be associated with a small barrier. This conclusion is supported by experiments that demonstrate a distinctively higher stability of model dimer cations where both pyrimidine rings are connected by a N1,N1′-thrimethylene linker, which restricts their mutual rotation.[8]

Solvent Effects: Charge and Spin Transfer. Experimentally, relatively strong solvent effects were found for the dissociation of pyrimidine dimer anions.[38] Thus, it seems desirable to investigate solvent effects also for the splitting reaction of dimer cations. The SCRF method applied is able to account for the electrostatic contribution to the solvation energy. This should be the most important effect of a polar medium (water) on the energetic characteristics of the splitting reaction, in particular in the present case where a cation is ultimately separated into an ion−dipole complex. To illustrate such solvent effects on the most reliable reaction profile, we corrected the B3LYP//UHF energies using solvation energies estimated at the B3LYP level (Table 2). The calculated solvation energies are collected in Table 3.

All structures involved in the dimer splitting process apparently undergo a relatively strong stabilization (by about 35−50 kcal/mol) due to interaction with a polar (aqueous) environment. In the Onsager reaction field model, which forms the basis for the present reaction field modeling of solvent effects, the solvent stabilization effect depends on the cavity radius and the molecular dipole moment.[34] For a charged system, a Born charge term has to be taken into account and the dipole moment has to be calculated with the respect to the center of electric charge.[34,35] The more symmetrical the electron charge distribution, the smaller is the dipole moment, hence the weaker the interaction with the solvent. Thus, the substantial decrease in the dipole moment when going from INT1 to INT2 (Table 3) is responsible for the significant lowering of the solvation energy accompanying this step (Table 3). The dipole moments related to each of the two rings have almost the same direction in INT1 but partially cancel each other in INT2. Also, a stronger localization of charge with the conformation remaining essentially unchanged should lead to a larger dipole moment. Indeed, comparing INT1 to TS3 or INT2 to TS4, one notes a

concomitant decrease in charge localization and dipole moment (Table 3). Therefore, one may expect that the energy difference between these configurations decreases with solvent polarity (Table 2 and Figure 2D). Similarly, the complete charge localization at one of the monomers is responsible for the stronger solvent stabilization of the separated monomers than that of the product complex (Table 3).

A clear picture of the course of the splitting process emerges from the analysis of the solvent effect on the reaction energy profile (Figure 2D). Along reaction path I the splitting process proceeds smoothly, without any activation barrier, from the unrelaxed initial state $U<>U^+_{NR}$ to the product complex PC. In contrast to the findings for the dimer radical anion,[38] a polar solvent does not reduce the dissociation efficiency of a pyrimidine dimer cation. On the contrary, due to the increased exothermicity of the overall process $U<>U^+_{NR} \rightarrow U + U^+$, the thermodynamic driving force facilitates the splitting reaction in polar media. In fact, the solvent stabilization is significantly larger for the separated monomers than for the unrelaxed cation; see Table 3. Similar to reaction path I, there is also no activation barrier along path II connected with the cleavage of the C5−C5′ bond (see the negative value of E_a associated with INT2, Table 2). On the other hand, the rotational barrier of reaction path II, when going from INT1 via TS2 to INT2, increases even with solvent polarity. Thus, a polar solvent should favor reaction path I even more.

As we have seen, solvent effects are connected to charge separation and intramolecular charge transfer along the reaction path. During the structural relaxation to $U<>U^+$ both charge and spin density are almost equally delocalized over both rings. On the way to the intermediate, the C6−C6′ one-electron bond is broken in such a way that charge and spin become localized at opposite rings 1 and 1′, respectively (Table 3). The last step of the cleavage reaction is most interesting. Namely, the C5−C5′ bond breaks in TS4, that is, on reaction path I, in heterolytic fashion; the associated electron pair is moved as a whole to ring 1. As a result, ring 1 becomes a neutral uracil molecule while ring 1′ is converted into a uracil cation (Table 3). This course of the process is probably forced by the relative orientation of both rings, since after a heterolytic bond breakage the negative end of the molecular dipole of the neutral uracil molecule is closer to the uracil cation than in the situation resulting after a homolytic C5−C5′ bond cleavage. The former process directly leads to complex PC′, which due to its structure, is conceivable only for a dimer system without any constraints. On reaction path II the cleavage of the C5−C5′ bond proceeds via symmetric transition state TS3 but in the same heterolytic fashion. In DNA, homolytic splitting of the C5−C5′ bond is more plausible due to geometry constraints as was described previously.[15] Thus, the pyrimidine dimer cleavage can be considered as an important example for a reaction that features a high sensitivity toward conformational flexibility of the overall system.

Conclusions

We have presented a computational investigation of the splitting reaction of a uracil dimer radical cation, using Hartree−Fock and correlated methods. The study unambiguously established the important role of dynamic correlation effects on the predicted reaction mechanism. The features of the HF and DF potential-energy surfaces differ noticeably, although both surfaces are in line with the experimental finding concerning the extremely low stability of the pyrimidine dimer cation. While at the HF level the reaction proceeds through an intermediate state separated by saddle points from the reactant and the products, no barriers are found at a the B3LYP level when proceeding along reaction path I. On reaction path II, the activation barrier associated with a rotational transformation of INT1 into INT2 remains even at the correlated level of theory. Thus, although INT2 is more stable than INT1, the splitting process will preferentially proceed along path I. Moreover, correlation considerably affects the reaction energy; the overall exothermicity calculated for the reaction $U<>U^+_{NR} \rightarrow U + U^+$ equals −15.1 and −33.5 kcal/mol at the B3LYP and HF levels of theory, respectively.

Our DF calculations also indicate that the splitting process may proceed with a rather small activation barrier if conformational constraints are applied, corroborating similar CASSCF reults.[15] This finding has direct bearing on the possibility for dimer cleavage in damaged DNA. It also rationalizes the higher experimental stability of linked model dimer cations.[8] Finally, we note that solvation of the photodimer radical cation in a polar medium leads to a more gradual release of the reaction energy along the path to the ion−molecule product complex, but the qualitative picture of the reaction profile, as obtained from gas-phase calculations, does not change as long as one considers path I and path II separately. However, comparison of both paths leads to the conclusion that path II is even less probable in a polar solvent than in the gas phase. Namely, with increasing solvent polarity the rotational barrier (TS2) becomes higher and INT1 becomes more stable than INT2. Finally, it is also worth noting that the exothermicity of the overall dimer splitting process to the ion−dipole complex increases significantly in a polar solvent.

Acknowledgment. J.R. is grateful to the Alexander von Humboldt Foundation for a fellowship. This work has been supported by the Deutsche Forschungsgemeinschaft through SFB 377 and by the Fonds der Chemischen Industrie.

References and Notes

(1) Kim, S.-T.; Sancar, A. *Photochem. Photobiol.* **1993**, *57*, 895.
(2) Hartman, F. R.; Van Camp, J. R.; Rose, S. D. *J. Org. Chem.* **1987**, *52*, 2684.
(3) Heelis, P. F.; Kim, S.-T.; Okamura, T.; Sancar, A. *J. Photochem. Photobiol., B* **1993**, *17*, 219.
(4) Heelis, P. F.; Hartman, R. F.; Rose, S. D. *Chem. Soc. Rev.* **1995**, 289.
(5) Sancar, A. *Biochemistry* **1994**, *33*, 2.
(6) Epple, E.; Wallenborn, E.-U.; Carell, T. *J. Am. Chem. Soc.* **1997**, *119*, 7440.
(7) Begley, T. P. *Acc. Chem. Res.* **1994**, *27*, 394.
(8) Pouwels, P. J. W.; Hartman, R. F.; Rose, S. D.; Kaptein, R. *Photochem. Photobiol.* **1995**, *61*, 563; 575.
(9) Heelis, P. F.; Hartman, R. F.; Rose, S. D. *J. Photochem. Photobiol. A* **1996**, *95*, 89.
(10) Scannell, M. P.; Fenick, D. J.; Yeh, S.-Y.; Falvey, D. E. *J. Am. Chem. Soc.* **1997**, *119*, 1971.
(11) Voityuk, A. A.; Michel-Beyerle, M.-E.; Rösch, N. *J. Am. Chem. Soc.* **1996**, *118*, 9750.
(12) Voityuk, A. A.; Rösch, N. *J. Phys. Chem. A* **1997**, *101*, 8335.
(13) Dandliker, P. J.; Holmlin, R. E.; Barton, J. K. *Science* **1997**, *275*, 1465.
(14) Aida, M.; Kaneko, M.; Dupuis, M. *Int. J. Quantum Chem.* **1996**, *57*, 949.
(15) Aida, M.; Inoue, F.; Kaneko, M.; Dupuis, M. *J. Am. Chem. Soc.* **1997**, *119*, 12274.
(16) Jungwirth, P.; Carsky, P.; Bally, T. *J. Am. Chem. Soc.* **1993**, *115*, 5776.
(17) Baker, J.; Muir, M.; Andzelm, J. *J. Chem. Phys.* **1995**, *102*, 2063.
(18) Torrent, M.; Duran, M.; Sola, M. *J. Mol. Struct: THEOCHEM* **1996**, *362*, 163.
(19) Jursic, B. S. *Int. J. Quantum Chem.* **1997**, *65*, 75.
(20) Bottoni, A. *J. Chem. Soc., Perkin Trans. 2* **1996**, 2041.

(21) Bach, R. D.; Glukhovtsev, M. N.; Gonzalez, C.; Marquez, M.; Estevez, C. M.; Baboul, A. G.; Schlegel, H. B. *J. Phys. Chem. A* **1997**, *101*, 6092.

(22) Jursic, B. S. In *Theoretical and Computational Chemistry*; Seminario, J. M., Ed.; Elsevier: Amsterdam, 1996; Vol. 4, p 709.

(23) Parr, R. G.; Yang, W. *Density-Functional Theory of Atoms and Molecules*; Oxford University Press: New York, 1989.

(24) Becke, A. D. *Phys. Rev. A* **1988**, *37*, 785.

(25) Becke, A. D. *J. Chem. Phys.* **1993**, *98*, 5648.

(26) Lee, C.; Yang, W.; Parr, R. G. *Phys. Rev. B* **1988**, *41*, 785.

(27) Curtiss, L. A.; Raghavachari, K.; Redfern, P. C.; Pople, J. A. *J. Chem. Phys.* **1997**, *106*, 1063.

(28) Frisch, M. J.; Trucks, G. W.; Schlegel, H. B.; Gill, P. M. W.; Johnson, B. G.; Robb, M. A.; Cheeseman, J. R.; Keith, T.; Petersson, G. A.; Montgomery, J. A.; Raghavachari, K.; Al-Laham, M. A.; Zakrzewski, V. G.; Ortiz, J. V.; Foresman, J. B.; Cioslowski, J.; Stefanov, B. B.; Nanayakkara, A.; Challacombe, M.; Peng, C. Y.; Ayala, P. Y.; Chen, W.; Wong, W. M.; Andres, J. L.; Replogle, E. S.; Gomperts, R.; Martin, R. L.; Fox, D. J.; Binkley, J. S.; Defrees, D. J.; Baker, J.; Stewart, J. P.; Head-Gordon, M.; Gonzalez, C.; Pople, J. A. *Gaussian 94*, revision D.4; Gaussian, Inc.: Pittsburgh, PA, 1995.

(29) Hariharan, P. C.; Pople, J. A. *Theor. Chim. Acta* **1973**, *28*, 213.

(30) Schlegel, H. B. In *New Theoretical Concepts for Understanding Organic Reactions*; Bertran, J., Ed.; Kluwer Academic: Dordrecht, 1989; p 33.

(31) Peng, C. Y.; Ayala, P. Y.; Schlegel, H. B.; Frisch, M. J. *J. Comput. Chem.* **1996**, *17*, 49.

(32) Hehre, W. J.; Radom, L.; Schleyer, P. v. R.; Pople, J. A. *Ab Initio Molecular Orbital Theory*; Wiley: New York, 1986.

(33) Boys, S. F.; Bernardi, F. *Mol. Phys.* **1970**, *19*, 553.

(34) Tomasi, J.; Persico, M. *Chem. Rev.* **1994**, *94*, 2027.

(35) Wong, M. W.; Frisch, M. J.; Wiberg, K. B. *J. Am. Chem. Soc.* **1991**, *113*, 4776.

(36) Sponer, J.; Leszczynski, J.; Hobza, P. *J. Phys. Chem.* **1996**, *100*, 5590.

(37) Thiel, W. *Adv. Chem. Phys.* **1996**, *43*, 703.

(38) Kim, S.-T.; Rose, S. D. *J. Photochem. Photobiol. B* **1992**, *12*, 179.